Proceedings of the ASME 2011 30th International Conference on Ocean, Offshore and Arctic Engineering
OMAE2011
June 19-24, 2011, Rotterdam, The Netherlands

OMAE2011-49057

FLUID-STRUCTURE ENERGY TRANSFER OF A TENSIONED BEAM SUBJECT TO VORTEX-INDUCED VIBRATIONS IN SHEAR FLOW

Rémi Bourguet*
Massachusetts Institute of Technology
Cambridge, MA, USA
Email: bourguet@mit.edu

Michael S. Triantafyllou
Massachusetts Institute of Technology
Cambridge, MA, USA
Email: mistetri@mit.edu

Michael Tognarelli
BP America Production Co.
Houston, TX, USA
Email: michael.tognarelli@bp.com

Pierre Beynet
BP America Production Co.
Houston, TX, USA
Email: pierre.beynet@bp.com

ABSTRACT

The fluid-structure energy transfer of a tensioned beam of length to diameter ratio 200*, subject to vortex-induced vibrations in linear shear flow, is investigated by means of direct numerical simulation at three Reynolds numbers, from* 110 *to* 1,100*. In both the in-line and cross-flow directions, the high-wavenumber structural responses are characterized by mixed standing-traveling wave patterns.*

The spanwise zones where the flow provides energy to excite the structural vibrations are located mainly within the region of high current where the lock-in condition is established, i.e. where vortex shedding and cross-flow vibration frequencies coincide. However, the energy input is not uniform across the entire lock-in region. This can be related to observed changes from counter-clockwise to clockwise structural orbits. The energy transfer is also impacted by the possible occurrence of multi-frequency vibrations.

INTRODUCTION

Long flexible cylindrical structures immersed in cross-flow exhibit Vortex-Induced Vibrations (VIV). Such vibrations are an important issue for ocean engineering applications as they may lead to fatigue failure of tubular members such as risers placed within sheared ocean currents. In this context, the reliable estimation of the structural fatigue damage requires detailed understanding and efficient prediction of these self-excited oscillations.

Most of VIV studies have focused on the simplified problems of a rigid circular cylinder free to move or forced to oscillate in the cross-flow direction, in uniform current. These works have contributed to elucidate some fundamental VIV mechanisms as reviewed in Bearman (1984); Sarpkaya (2004); Williamson & Govardhan (2004). In particular, it appears that large amplitude oscillations occur when the vortex shedding and the structural vibration frequencies coincide, a condition referred to as 'lock-in'.

Despite its implications in the domain of applications, the case of long flexible cylinders has attractred less attention, especially for beams in sheared currents. Field and laboratory experiments on long tensioned beams free to oscillate in non-uniform flows highlighted the mixed standing-traveling wave nature of the vibrations, involving high structural wavenumbers and, often, multiple frequencies of response (e.g. Trim *et al.*, 2005; Lie & Kaasen, 2006; Vandiver *et al.*, 2009). Such features have also been analyzed through numerical simulations at moderate Reynolds number (Lucor *et al.*, 2006). These studies have focused on a quantification of the structural response, but did not

*Address all correspondence to this author.

provide information concerning the occurrence of the lock-in condition and the mechanisms of structure excitation. The effect of the possible multi-frequency nature of the vibrations on the fluid-structure interaction processes has to be investigated. In addition, the orientation of the cylinder orbits can influence the regularity of its trajectories (Dahl *et al.*, 2007) and may also be related to the occurrence of the lock-in condition along the span (Vandiver *et al.*, 2009; Modarres-Sadeghi *et al.*, 2010). However, its possible impact on the energy transfer between the flow and the structure is still unclear.

On the basis of a joint analysis of the vibrational responses and flow patterns, the objective of this work is to shed light on the fluid-structure energy transfer and especially on the mechanisms of long flexible cylinder excitation in non-uniform flow. We employ direct numerical simulation to predict the VIV of a long tensioned beam of length to diameter aspect ratio 200, immersed in a linear shear flow, in the range of Reynolds numbers $110-1{,}100$, so as to include the transition to turbulence in the wake.

The physical model and numerical method are briefly described in a first section. The structural vibrations are quantified in a second section. The occurrence of the lock-in condition is examined in a third section and the fluid-structure energy transfer are analyzed in a fourth section. The main findings of this study are summarized in a fifth section.

PHYSICAL MODEL AND NUMERICAL METHOD

The flow past a flexible cylinder of circular cross-section is predicted using direct numerical simulation of the three-dimensional incompressible Navier-Stokes equations. The cylinder is submitted to an oncoming flow which is parallel to the global x axis and linearly sheared along the global z axis, as illustrated in Fig. 1. In the following, all physical variables are non-dimensionalized using the cylinder diameter D and the maximum inflow velocity U, which occurs at $z=0$. The ratio between maximum and minimum inflow velocity is equal to 3.67. The Reynolds number (Re) is based on D and the inflow velocity. Three Re ranges are considered: Re$\in[30,110]$, Re$\in[90,330]$ and Re$\in[300,\ 1{,}100]$. The three corresponding simulations are denoted by the maximum Reynolds number Re$_m$.

The cylinder aspect ratio is $L/D=200$, where L is the cylinder length in its equilibrium position in quiescent flow. It is pinned at both ends, while it is free to move in both the in-line (x) and cross-flow (y) directions. The cylinder mass ratio is defined as $m=\rho_c/\rho_f D^2$, where ρ_c is the cylinder mass per unit length, and ρ_f the fluid density (Newman & Karniadakis, 1997). The actual ratio between the mass of the cylinder and the mass of the displaced fluid is equal to $4m/\pi$. The mass ratio is set equal to 6. The constant tension, bending stiffness and damping of the structure are designated by T, EI and K, respectively. The in-line and cross-flow displacements of the cylinder are denoted by

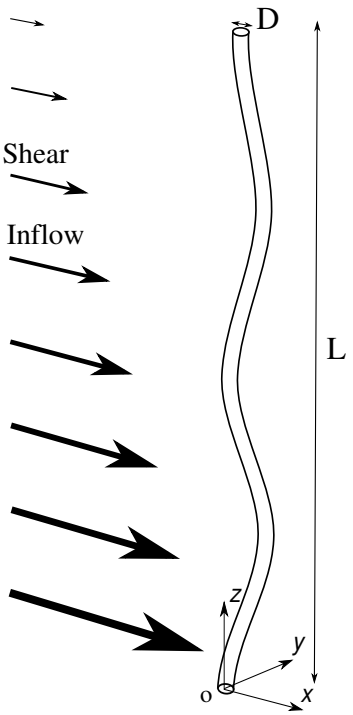

FIGURE 1. SKETCH OF THE PHYSICAL CONFIGURATION.

ζ_x and ζ_y. The sectional drag and lift coefficients are defined as $C_x=2F_x/\rho_f DU^2$ and $C_y=2F_y/\rho_f DU^2$, where F_x and F_y are the in-line and cross-flow dimensional fluid forces. The structural dynamics are governed by a tensioned beam model, expressed as follows in non-dimensional form (Evangelinos & Karniadakis, 1999):

$$\frac{\partial^2\zeta}{\delta t^2}-\omega_c^2\frac{\partial^2\zeta}{\delta z^2}+\omega_b^2\frac{\partial^4\zeta}{\delta z^4}+\frac{K}{m}\frac{\partial\zeta}{\delta t}=\frac{1}{2}\frac{C}{m}, \qquad (1)$$

where $\zeta=[\zeta_x,\zeta_y]^T$ and $C=[C_x,C_y]^T$. t denotes the non-dimensional time variable. ω_c and ω_b are the cable and beam phase velocities, defined as $\omega_c^2=T/m$ and $\omega_b^2=EI/m$, respectively. The structural damping is set equal to zero ($K=0$) to allow maximum amplitude oscillations. A tensioned beam is considered in this study, with $\omega_c=4.55$ and $\omega_b=9.09$. These structural parameters lead to vibrations involving high structural wavenumbers, which are representative of configurations encountered in the context of ocean engineering.

The parallelized code *Nektar*, based on the spectral/*hp* element method (Karniadakis & Sherwin, 1999), is used to solve the coupled fluid-structure system. Details regarding validation studies of the numerical method and parameters have been reported in Newman & Karniadakis (1997) and Evangelinos & Karniadakis (1999). The computational domain extends $50D$ downstream and $20D$ in front, above, and below the cylinder.

A two-dimensional grid of 2175 elements with polynomial order $p = 6$ or $p = 7$, depending on the Reynolds number, is used in the (x,y) planes. In the z direction, 512 planes (256 complex Fourier modes) are used for the $\mathrm{Re}_m = 110$ case, and 1024 planes (512 complex Fourier modes) in the $\mathrm{Re}_m = 330$ and $\mathrm{Re}_m = 1{,}100$ cases. The spatial resolution is similar to Evangelinos & Karniadakis (1999)'s study for a cylinder of aspect ratio $L/D = 4\pi$ constrained to oscillate in cross-flow direction, at Re$=$ 1,000. A buffer region of 8% of the cylinder length ($16D$) is defined, where the inflow velocity profile is adjusted to satisfy the spanwise periodicity boundary condition due to Fourier expansion (Lucor *et al.*, 2006). The buffer region is not shown in the following. Numerical tests on the boundary conditions, computational domain and buffer region sizes have been performed. The results reported in this study are based on time series of more than 300 convective time units, collected after the initial transient dies out, for each Re_m.

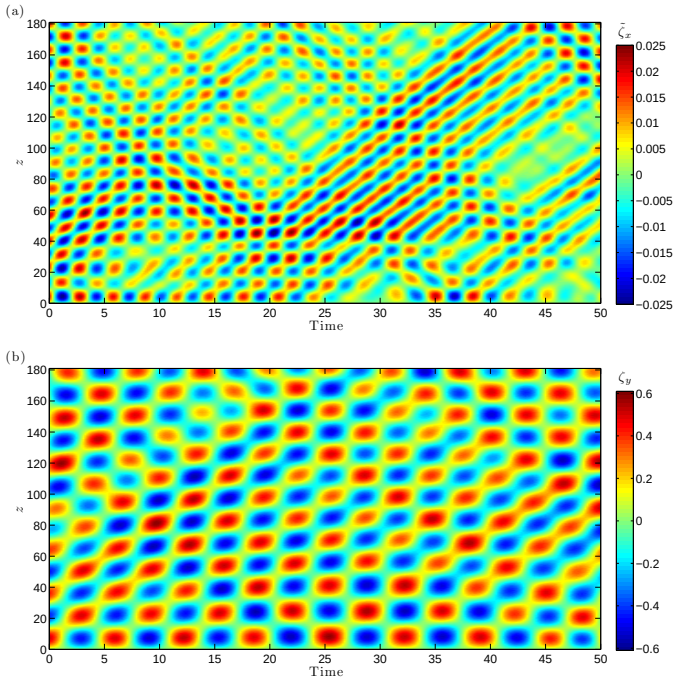

FIGURE 2. TEMPORAL EVOLUTION OF (a) IN-LINE DISPLACEMENT FLUCTUATION AND (b) CROSS-FLOW DISPLACEMENT ALONG THE CYLINDER SPAN, AT $\mathrm{Re}_m = 330$.

STRUCTURAL VIBRATIONS

In both the in-line and cross-flow directions, the structural response is a combination of standing and traveling wave patterns, as illustrated in Fig. 2 by the spatio-temporal evolution of the in-line displacement fluctuation and cross-flow displacement over a selected time interval, at $\mathrm{Re}_m = 330$. The traveling components of the vibrations are more pronounced in the in-line direction and principally oriented from the high to low inflow velocity regions (increasing z). Standing wave patterns dominate in the region near $z = 0$ in both directions until approximately $z = 30$.

RMS values of the vibration amplitudes reflect the mixed nature of the responses (Fig. 3). In these plots and in the following, only the deviations of the in-line motion from its mean value, $\tilde{\zeta}_x$, are considered. The standing character of the responses leads to the formation of cells along the span corresponding to alternating 'nodes' (minima of the response envelope) and 'anti-nodes' (maxima of the response envelope). Despite the shear flow, the displacements associated with anti-nodes remain relatively constant along the cylinder span. The RMS values of the displacements associated with nodes are different from zero because of the superimposed traveling wave components. The Re_m influence on response amplitudes is more pronounced in the in-line direction. The amplitudes of vibration reached at $\mathrm{Re}_m = 1{,}100$ are similar to experimental measurements carried out with flexible cylinders at higher Reynolds numbers (Trim *et al.*, 2005; Chaplin *et al.*, 2005; Lie & Kaasen, 2006; Huera-Huarte & Bearman, 2009).

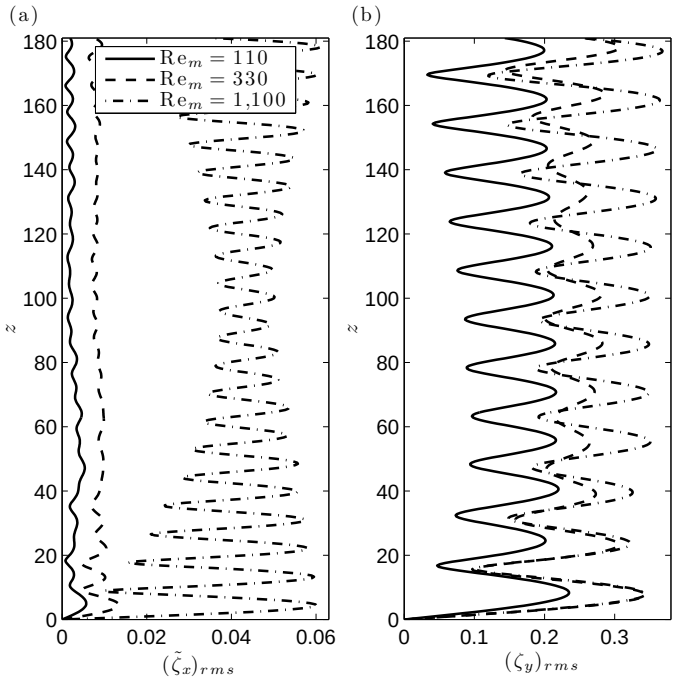

FIGURE 3. RMS VALUE OF (a) IN-LINE DISPLACEMENT FLUCTUATION AND (b) CROSS-FLOW DISPLACEMENT ALONG THE CYLINDER SPAN. THE MAXIMUM INFLOW VELOCITY OCCURS AT $z = 0$.

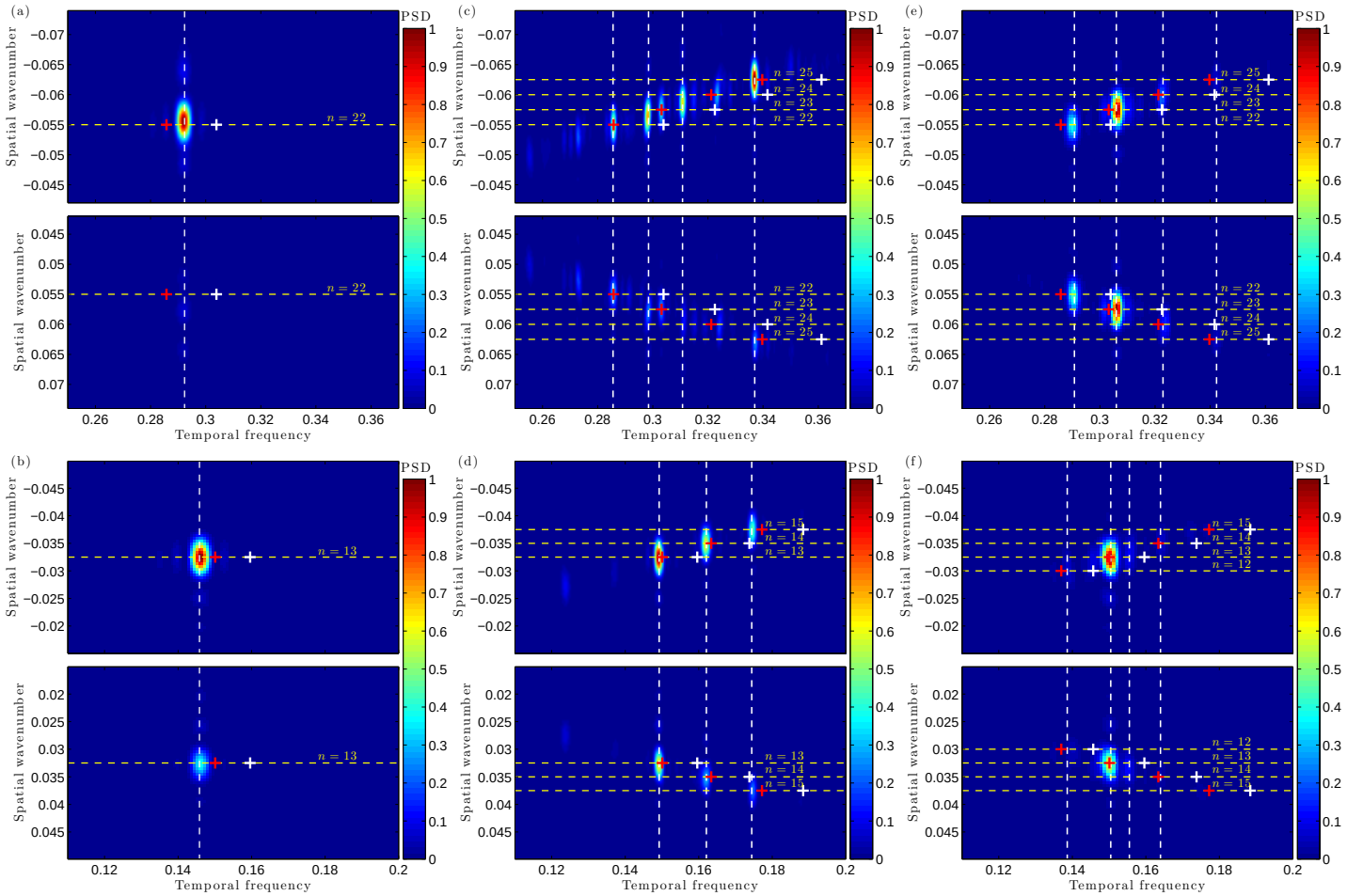

FIGURE 4. SPATIO-TEMPORAL SPECTRAL ANALYSIS OF (a,c,e) IN-LINE DISPLACEMENT FLUCTUATION AND (b,d,f) CROSS-FLOW DISPLACEMENT AT (a,b) $\mathrm{Re}_m = 110$, (c,d) $\mathrm{Re}_m = 330$, (e,f) $\mathrm{Re}_m = 1{,}100$. WHITE VERTICAL DASHED LINES DENOTE PREDOMINANT FREQUENCIES. WAVENUMBERS OF SELECTED SINE FOURIER MODES ARE INDICATED BY YELLOW HORIZONTAL DASHED LINES. WHITE (RED) CROSSES DENOTE NATURAL (MODIFIED) FREQUENCIES ASSOCIATED WITH THESE WAVENUMBERS.

Spatio-temporal spectral analysis is carried out to clarify the nature of the structural vibrations. This is achieved by a two-dimensional FFT of the spatio-temporal evolution of the structural responses which are zero padded to reach a frequency resolution of 5×10^{-4} in both time and space. In Fig. 4, Power Spectral Densities (PSD) of the in-line and cross-flow displacements are plotted as functions of temporal frequency and spatial wavenumber. Positive frequencies are presented and thus negative wavenumbers (upper part of each plot) are associated with traveling waves moving towards the low velocity region while positive wavenumbers (lower part of each plot) represent traveling waves moving towards the high velocity region. PSD are normalized by the maximum observed on both domains (positive and negative wavenumbers) to illustrate the traveling or standing character of the response. The predominant vibration frequencies are identified by white vertical dashed lines. Sine Fourier modes ($\sin(\pi nzD/L)$ for the n^{th} mode) are often used to describe the structural response (e.g. Chaplin *et al.*, 2005; Lie & Kaasen, 2006). For illustration purposes, and comparison with the existing literature, the wavenumbers corresponding to selected sine Fourier modes are indicated by yellow horizontal dashed lines.

Responses at a single frequency as well as responses at several frequencies can be observed along the span. These two types of response are referred to as 'mono-frequency' and 'multi-frequency', respectively. In the case of multi-frequency response, as, for instance, in the in-line direction at $\mathrm{Re}_m = 330$, it can be noticed that the peaks are clearly defined and distinct from each other, despite a narrow-band vibration, in the range of $[0.24, 0.36]$. The ratio between the in-line and cross-flow excited frequencies is generally close to 2, including the multi-frequency cases.

The predominant excited wavenumbers correspond to

modes $n \in \{22,23,24,25\}$ in the in-line direction and $n \in \{13,14,15\}$ in the cross-flow direction. These mode numbers are close to those measured experimentally by Trim *et al.* (2005) and Lie & Kaasen (2006), where cases of multi-frequency response have been reported in shear flow. It is recalled that in the present case of mixed standing-traveling wave reponses, the concept of structural modes is used loosely, for illustration purposes only. In all cases, the ratio between the in-line and cross-flow excited wavenumbers is different from 2 as expected, since for a mixed cable/beam structure, the relation between a spatial wavenumber and the corresponding natural frequency is not linear.

In general, at a given vibration frequency it appears that only a single peak emerges in the spatial spectrum, at the same wavenumber on both the negative and positive sides; i.e. a single structural wavelength is excited at a given frequency. As expected for a tensioned beam, the excited structural wavenumber increases with increasing excitation frequency. The natural frequency f^{nat} of the tensioned beam associated with the wavenumber k can be evaluated as follows, in vacuum:

$$f^{\text{nat}}(k) = k\sqrt{\omega_c^2 + 4\pi^2\omega_b^2 k^2}. \tag{2}$$

The frequencies corresponding to the selected wavenumbers are indicated by white crosses in Fig. 4. The effective vibration frequencies present a strong drift from the natural frequency spectrum. This spectrum can be modified as follows to take into account the immersion of the cylinder into the fluid:

$$f^{\text{mod}} = f^{\text{nat}}\sqrt{\frac{m}{m+\frac{\pi}{4}C_m}}, \tag{3}$$

where C_m is the added mass coefficient induced by the fluid. The corresponding modified frequencies f^{mod}, for a choice of $C_m = 1$, are indicated by red crosses in Fig. 4. While this modified spectrum seems to provide a reasonable approximation to the effective excited frequencies in some cases, significant discrepancies appear in other cases which emphasizes the variability of the added mass coefficient, and hence the difficulty of estimating a priori the structural response.

The relative weights of negative and positive wavenumber peaks for the same frequency confirm the observations made previously concerning the mixed standing-traveling character of structural vibrations and, especially, the preferential orientation of the traveling wave components from high to low inflow velocity regions.

LOCK-IN WITHIN SHEAR FLOW

In the case of flexibly-mounted rigid cylinders in uniform flow, the phenomenon of lock-in consists of self-excited, vortex-induced vibrations accompanied by the synchronization of the

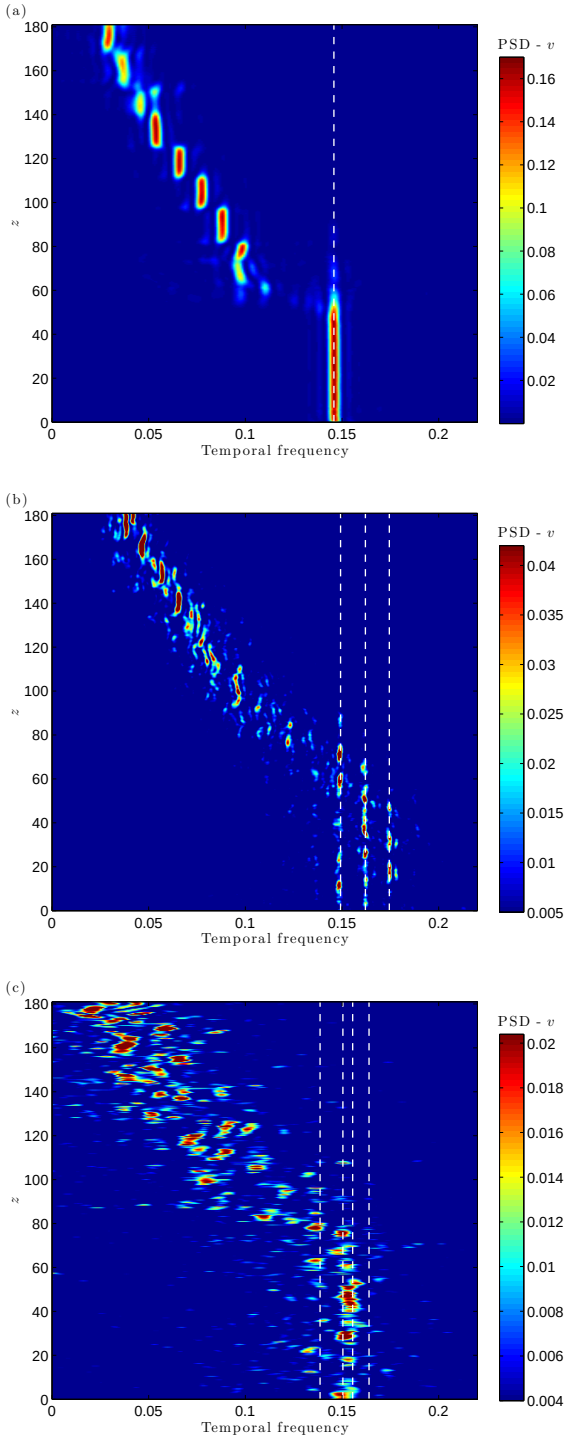

FIGURE 5. PSD OF THE TEMPORAL EVOLUTION OF CROSS-FLOW COMPONENT OF FLOW VELOCITY ALONG A SPANWISE LINE LOCATED AT $(x,y) = (20,0)$, AT (a) $\text{Re}_m = 110$, (b) $\text{Re}_m = 330$, (c) $\text{Re}_m = 1{,}100$. DASHED LINES INDICATE PREDOMINANT FREQUENCIES OF STRUCTURE VIBRATION.

frequency of vortex formation with the frequency of cylinder vibration. The lock-in phenomenon has been extensively investigated in this context (Bearman, 1984; Sarpkaya, 2004; Williamson & Govardhan, 2004).

In the context of long flexible cylinders in shear flow, the lock-in condition can be defined locally; at each spanwise location, the lock-in condition is established when the local vortex shedding frequency coincides with the local cross-flow vibration frequency. The corresponding frequency is the local lock-in frequency. In the absence of such synchronization, the condition is referred to as non-lock-in. The spanwise region which includes all the locally locked-in locations is referred to as the lock-in region and the rest of the span as the non-lock-in region.

The vortex shedding frequency is quantified from the cross-flow component of the flow velocity, v, along a spanwise line located downstream of the cylinder at $(x,y) = (20,0)$. The PSD of the v velocity component is plotted along the span for the three Re_m in Fig. 5. The predominant cross-flow vibration frequencies determined in Fig. 4 are indicated by white dashed lines.

In all cases, a region of lock-in can be identified in the high oncoming flow velocity zone, near $z = 0$. The rest of the span corresponds to a non-lock-in region, where the vortex shedding and the structural vibrations are not synchronized. The lock-in region covers $59D$, $75D$ and $77D$ at $\mathrm{Re}_m = 110$, $\mathrm{Re}_m = 330$ and $\mathrm{Re}_m = 1{,}100$, respectively. The case of $\mathrm{Re}_m = 330$ exhibits lock-in at all three distinct frequencies identified in the multi-frequency structural response. Despite some secondary contributions, it can be observed that, at each spanwise location, the vortex shedding is mainly synchronized with a single frequency, which can be different for each location. In addition, a comparison of the cross-flow vibration and flow velocity spectra shows that the locally predominant vibration frequency is preferred by the coupled-fluid structure system when establishing the lock-in condition. At $\mathrm{Re}_m = 1{,}100$, the spanwise evolution of the predominant frequency of v is more irregular than in other cases, due to the absence of stable wake patterns in several spanwise regions. These zones form 'holes' in the lock-in spanwise pattern.

FLUID-STRUCTURE ENERGY TRANSFER

The fluid-structure energy transfer is quantified by means of the force coefficient in phase with the cylinder velocity in a similar way as used in Newman & Karniadakis (1997), Hover *et al.* (1998) and Dahl *et al.* (2010). The present analysis includes both the in-line and cross-flow contributions of this coefficient. The time-averaged force coefficient in phase with the cylinder velocity is defined as:

$$C_{fv} = \frac{\sqrt{2}\langle \tilde{C}_x \dot{\tilde{\xi}}_x + C_y \dot{\xi}_y \rangle}{\sqrt{\langle \dot{\tilde{\xi}}_x^2 + \dot{\xi}_y^2 \rangle}}, \qquad (4)$$

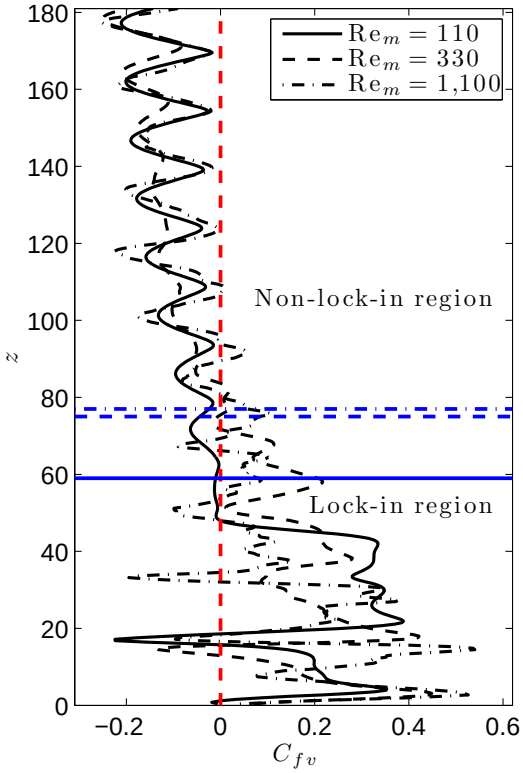

FIGURE 6. SPANWISE EVOLUTION OF THE FORCE COEFFICIENT IN PHASE WITH VELOCITY. BLUE HORIZONTAL LINES INDICATE THE LIMIT OF THE LOCK-IN REGION ISSUED FROM Fig. 5 (SAME LINE STYLES AS FOR C_{fv}).

where $\tilde{C}_x$ is the fluctuating part of C_x about its mean value, $\langle\cdot\rangle$ the time-averaging operator and $\dot{p}$ the time derivative of p. The lift and drag coefficients are based on the maximum oncoming flow velocity U ($z = 0$) so that C_{fv} is representative of the relative contribution of each spanwise location to the overall energy transfer. C_{fv} quantifies the power developed by the fluid acting on each section of the vibrating cylinder. Positive C_{fv} implies that the fluid supplies, on average, energy to the structure and hence excites cylinder vibration, while negative C_{fv} indicates that the fluid is damping the cylinder motion.

The spanwise distribution of C_{fv} is plotted in Fig. 6 for the three Re_m studied. The limits of the lock-in regions are indicated by blue horizontal lines. Regions of positive C_{fv} are located in the high velocity zone for all Re_m cases, corresponding principally to the lock-in regions. In the non-lock-in region, C_{fv} remains negative.

Within the lock-in region, C_{fv} exhibits large spanwise variations. Negative peaks can occur near the minima of the vibration envelope in all studied cases. C_{fv} can also be influenced by the orientation of the cylinder orbital motion in the (x,y) plane. The

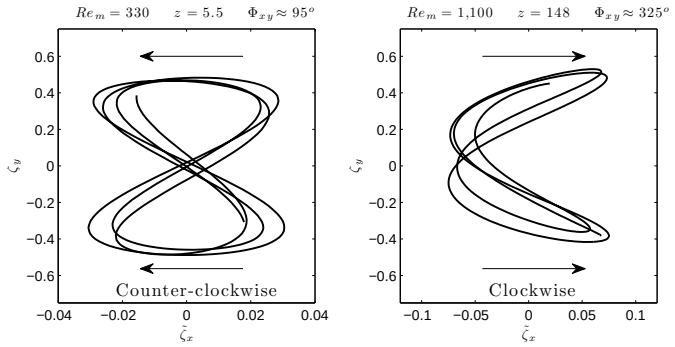

FIGURE 7. EXAMPLES OF COUNTER-CLOCKWISE AND CLOCKWISE TRAJECTORIES.

shape and orientation of the beam trajectories are controlled by the phase difference between the in-line and cross-flow displacements, which are non-linearly coupled by the fluid forces. The instantaneous phases of the in-line and cross-flow displacements (ϕ_x and ϕ_y respectively) are determined by means of the Hilbert transform. Adopting an approach similar to Huera-Huarte & Bearman (2009), the phase difference Φ_{xy} is evaluated as follows:

$$\Phi_{xy} = [p\phi_x - q\phi_y, \quad \mod 360^o], \tag{5}$$

where p and q are two integer numbers defining the level of synchronization studied. The couple $(p,q) = (1,2)$ is chosen here. Values of Φ_{xy} in the range $0^o - 180^o$ ($180^o - 360^o$ respectively) correspond to 'figure eight' orbits where the beam moves upstream (downstream respectively) when reaching the cross-flow oscillation maxima. These two types of trajectories are referred to as 'counter-clockwise' and 'clockwise' respectively (Dahl *et al.*, 2007). Examples of counter-clockwise and clockwise trajectories are plotted in Fig. 7.

Detailed views of the spanwise evolution of C_{fv} near $z = 0$ are plotted in Fig. 8, in the cases of mono-frequency ($\mathrm{Re}_m = 110$, Fig. 8(a)) and multi-frequency responses ($\mathrm{Re}_m = 330$, Fig. 8(c)). Fig. 8(b) and (d) represent the spanwise evolution of the histogram of phase difference Φ_{xy} between the in-line and cross-flow motions in the same region, in the corresponding cases. In both cases, a predominant trajectory can be identified at each spanwise location. Due to the pronounced standing wave component of the vibrations near $z = 0$, an alternating pattern of counter-clockwise and clockwise trajectories is observed in this zone, as z increases. It can be noticed that the passage from counter-clockwise to clockwise motion is accompanied by a reduction of C_{fv}. As a consequence, counter-clockwise trajectories appear more favorable to cylinder excitation, in both mono- and multi-frequency cases.

Within the non-lock-in region, C_{fv} exhibits a more regular spanwise pattern (Fig. 6): negative peaks are observed near vi-

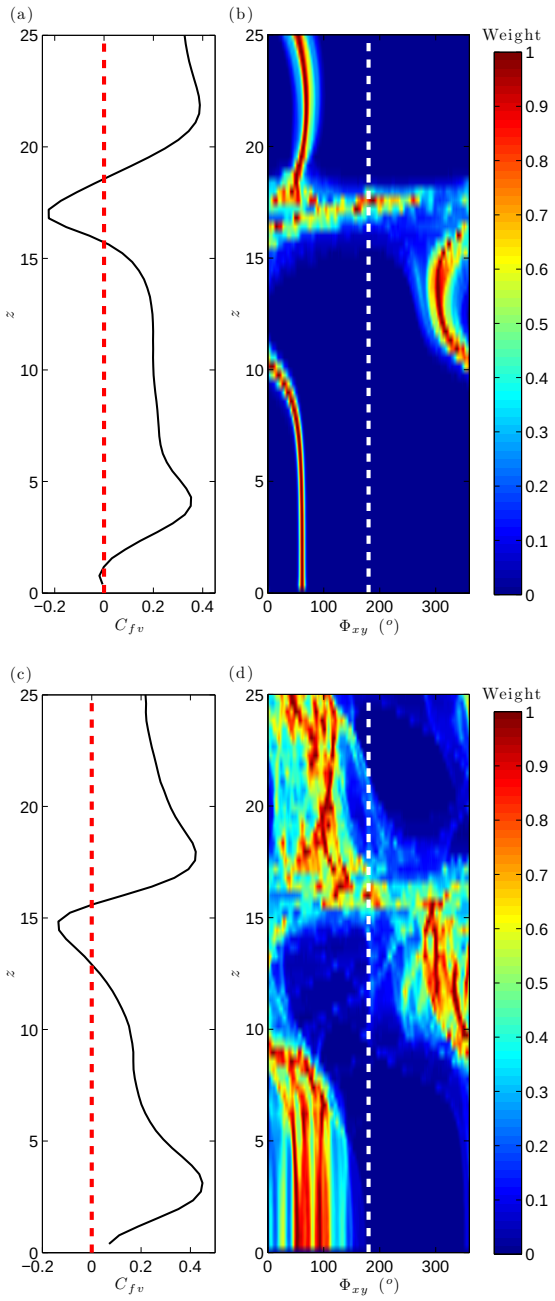

FIGURE 8. (a,c) FORCE COEFFICIENT IN PHASE WITH VELOCITY AND (b,d) HISTOGRAM OF IN-LINE/CROSS-FLOW MOTION PHASE DIFFERENCE ALONG THE CYLINDER SPAN (DETAIL NEAR $z = 0$), AT (a,b) $\mathrm{Re}_m = 110$ AND (c,d) $\mathrm{Re}_m = 330$.

bration anti-nodes and $C_{fv} \approx 0$ near vibration nodes.

A frequency decomposition of C_{fv} is presented in Fig. 9 to study the relation between lock-in/non-lock-in conditions and fluid-structure energy transfer in the case of multi-frequency vi-

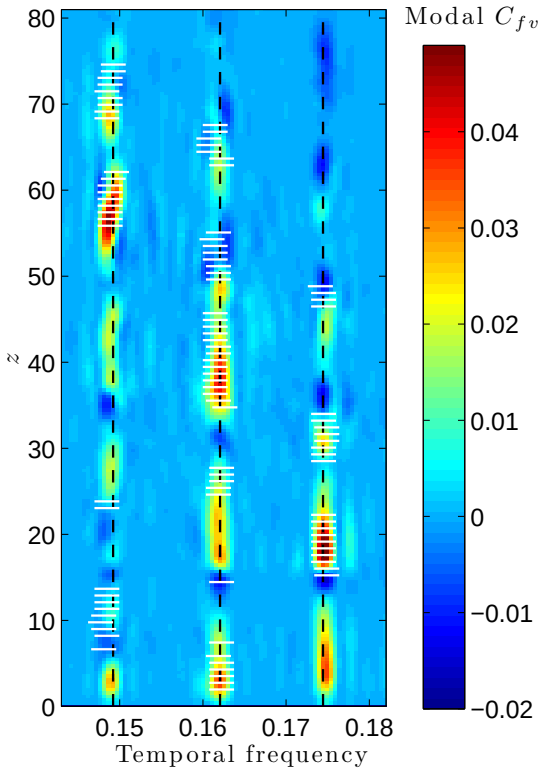

FIGURE 9. FREQUENCY DECOMPOSITION OF FORCE COEFFICIENT IN PHASE WITH VELOCITY ALONG THE CYLINDER SPAN (DETAIL OF THE LOCK-IN REGION), AT $\mathrm{Re}_m = 330$. BLACK DASHED LINES INDICATE THE PREDOMINANT FREQUENCIES OF THE CROSS-FLOW VIBRATION AND WHITE SEGMENTS INDICATE THE LOCAL LOCK-IN FREQUENCY.

brations ($\mathrm{Re}_m = 330$). Previously identified vibration frequencies are indicated by black dashed lines. In the case of multi-frequency response, it has been shown previously that lock-in occurs mainly at a single frequency at each spanwise location; as a consequence, positive energy transfer at each spanwise location is expected to occur mainly at this frequency. This is verified in Fig. 9, where white dashes are used to indicate the local predominant lock-in frequency as determined from Fig. 5(b): the main peaks of positive C_{fv} occur at the locally predominant lock-in frequencies.

SUMMARY

The in-line and cross-flow vortex-induced vibrations of a long tensioned beam immersed in a linearly sheared current have been predicted by means of direct numerical simulation, in the range of Reynolds numbers $110 - 1{,}100$, so as to include the transition to turbulence in the wake. The selected tension and bending stiffness lead to high-wavenumber vibrations, similar to those encountered in long ocean structures.

The structural response consists of a mixture of standing and traveling wave patterns in both the in-line and cross-flow directions; the traveling wave component is preferentially oriented from high to low oncoming flow velocity regions. Both mono-frequency and multi-frequency responses may be excited along the span. The local synchronization between the cross-flow vibration and vortex shedding frequencies, the lock-in condition, occurs in the high flow velocity region, over 30% or more of the cylinder span.

In the non-lock-in region, where vortex shedding and structure vibrations are not synchronized, the flow uniformly damps structural vibrations. In contrast, the flow does not uniformly excite structural vibrations within the lock-in region. In this region, the spanwise variability of the energy supplied by the flow to the structure can be associated with local changes in the orientation of the cylinder in-line/cross-flow trajectories. In both mono- and multi-frequency response cases, we find that orbits where the cylinder moves upstream at the extremes of cross-flow motion are more favorable to structure excitation.

In the case of multi-frequency vibrations, structural excitation occurs at multiple frequencies across the lock-in region. We find however that the lock-in appears as a locally mono-frequency event and hence the flow supplies energy to the structure mainly at the local lock-in frequency, i.e. the mechanism of excitation is that of locally mono-frequency excitation.

These results can provide insights for the development of VIV suppression or control techniques. They are also expected to influence the semi-empirical modeling efforts to predict VIV, which are based on short-span rigid cylinder hydrodynamic results.

ACKNOWLEDGMENT

Financial support was provided by the BP-MIT Major Projects Program and BP America Production Co.

REFERENCES

Bearman, P. W. 1984 Vortex shedding from oscillating bluff bodies. *Annual Review of Fluid Mechanics* **16**, 195–222.

Chaplin, J. R., Bearman, P. W., Huera-Huarte, F. J. & Pattenden, R. J. 2005 Laboratory measurements of vortex-induced vibrations of a vertical tension riser in a stepped current. *Journal of Fluids and Structures* **21**, 3–24.

Dahl, J. M., Hover, F. S., Triantafyllou, M. S., Dong, S. & Karniadakis, G. E. 2007 Resonant vibrations of bluff bodies cause multivortex shedding and high frequency forces. *Physical review letter* **99**, 144503.

Dahl, J. M., Hover, F. S., Triantafyllou, M. S. & Oakley, O. H. 2010 Dual resonance in vortex-induced vibrations at subcritical and supercritical Reynolds numbers. *Journal of Fluid Mechanics* **643**, 395–424.

Evangelinos, C. & Karniadakis, G. E. 1999 Dynamics and flow structures in the turbulent wake of rigid and flexible cylinders subject to vortex-induced vibrations. *Journal of Fluid Mechanics* **400**, 91–124.

Hover, F. S., Techet, A. H. & Triantafyllou, M. S. 1998 Forces on oscillating uniform and tapered cylinders in crossflow. *Journal of Fluid Mechanics* **363**, 97–114.

Huera-Huarte, F. J. & Bearman, P. W. 2009 Wake structures and vortex-induced vibrations of a long flexible cylinder part 1: Dynamic response. *Journal of Fluids and Structures* **25**, 969–990.

Karniadakis, G. E. & Sherwin, S. 1999 *Spectral/hp Element Methods for CFD*. Oxford: Oxford University Press.

Lie, H. & Kaasen, K. E. 2006 Modal analysis of measurements from a large-scale viv model test of a riser in linearly sheared flow. *Journal of Fluids and Structures* **22**, 557–575.

Lucor, D., Mukundan, H. & Triantafyllou, M. S. 2006 Riser modal identification in CFD and full-scale experiments. *Journal of Fluids and Structures* **22**, 905–917.

Modarres-Sadeghi, Y., Mukundan, H., Dahl, J. M., Hover, F. S. & Triantafyllou, M. S. 2010 The effect of higher harmonic forces on fatigue life of marine risers. *Journal of Sound and Vibration* **329**, 43–55.

Newman, D. J. & Karniadakis, G. E. 1997 A direct numerical simulation study of flow past a freely vibrating cable. *Journal of Fluid Mechanics* **344**, 95–136.

Sarpkaya, T. 2004 A critical review of the intrinsic nature of vortex-induced vibrations. *Journal of Fluids and Structures* **19**, 389–447.

Trim, A. D., Braaten, H., Lie, H. & Tognarelli, M. A. 2005 Experimental investigation of vortex-induced vibration of long marine risers. *Journal of Fluids and Structures* **21**, 335–361.

Vandiver, J. K., Jaiswal, V. & Jhingran, V. 2009 Insights on vortex-induced, traveling waves on long risers. *Journal of Fluids and Structures* **25**, 641–653.

Williamson, C. H. K. & Govardhan, R. 2004 Vortex-induced vibrations. *Annual Review of Fluid Mechanics* **36**, 413–455.